Imaging with cosmic-ray muons

1. Introduction

- When muons pass through a given material, lose their energy due to inelastic collisions with the atomic electrons and deflect from their incident direction due to elastic scattering from nuclei. Muons have very high penetration capabilities since they are least likely to interact with significant loss of energy. These characteristics qualify muons for the applications in imaging the objects of interest.
- **Muography** is an imaging technique based on the absorption or scattering of atmospheric muons.

2. The physics of muon radiography

- This technique is based on the measurement of the attenuation of the muon flux intensity by large massive object. The flux measurement is done downstream of the object to be investigated, i.e., after the muons have crossed it. This implies the possible use of just one muon tracker for imaging applications with this technique [1].
- Due to their interaction with the matter muons lose their energy proportionally to the ***length*** and to the ***mass density*** of the crossed rock.
- Considering a stretch of rock of length ***L*** with average mass density $\overline{\rho}$, the ***opacity X*** is defined as

$$X(L) = L\,\overline{\rho}, \text{ where } \overline{\rho} = \frac{1}{L}\int_L \rho(x)\,dx \qquad \textbf{(1)}$$

Applications:

1) Density distribution measurements:

- Opacity $X(\theta,\phi) = \frac{Numbers\ of\ muons\ passed\ the\ target\ of\ opacity\ X}{Number\ of\ muons\ without\ the\ target}$
- From the knowledge of the length of the rock ***L*(θ,ϕ)** and using the measured $X(\theta,\phi)$, $\overline{\rho}$**(θ,ϕ)** can be calculated from equation **(1)**.
- This technique has been applied to investigate volcanoes, hills, mineral deposits, pyramids, etc.

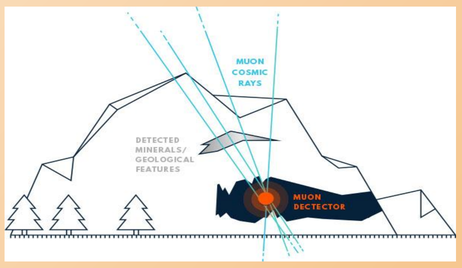

Figure 1: Geoscience applications using muon radiography [2].

2) Relative transmission for the detection of cavities:

- The transmission ***T* (θ,ϕ)** is defined as the fraction of muons that have been able to cross the object.
- The expected transmission T_E from a model:

$$T_E(\theta,\phi) = \frac{\int_{E^{min}(X)}^{\infty} \Phi(\theta,E)dE}{\int_{E^0}^{\infty} \Phi(\theta,E)dE}, \qquad \textbf{(2)}$$

- $E^{min}(X)$ - the minimum energy for a muon to cross the amount of rock of opacity X.
- E^0 - the minimum energy for a muon to be detected by the telescope.

- The measured transmission:

$$T_M(\theta,\phi) = \frac{\Delta T_{fs}}{\Delta T_u}\frac{N_\mu(\theta,\phi;X)}{N_{fs}(\theta,\phi)}, \qquad \textbf{(3)}$$

- $N_\mu(\theta,\phi;X)$ - number of muons measured in the presence of the object.
- $N_{fs}(\theta,\phi)$ - the free sky muons
- ΔT_u and ΔT_{fs} acquisition times.

- The relative transmission is $R(\theta,\phi) = \frac{T_M(\theta,\phi)}{T_E(\theta,\phi)}$ ⇨ If no void: $T_M(\theta,\phi) = T_E(\theta,\phi)$ ⇨ $R(\theta,\phi) \sim 1$ **OR** If there is a void: $T_M(\theta,\phi) > T_E(\theta,\phi)$ ⇨ $R(\theta,\phi) > 1$
- This technique has been applied to investigate cavities present in the railway tunnels.

3. The physics of muon tomography

- When the cosmic-ray muons crossing a given material, they are affected with elastic multiple Coulomb scattering from nuclei and deflect from the original traverse direction. After traversing a macroscopic amount of material, the net angular distribution features an approximately Gaussian core and the standard deviation can be expressed as

$$\sigma(\theta) = \frac{13.6\ MeV}{\beta cp}\sqrt{\frac{x}{X_0}}\left[1 + 0.038\ ln\frac{x}{X_0\beta^2}\right], \qquad \textbf{(4)}$$

where, p is the muon momentum, x is the path length from entry to exit, and X_0 is the radiation length [1]. A compact formula for $\frac{1}{X_0}$ is

$$\frac{1}{X_0} \propto \frac{Z(Z+1)}{A}\,ln\left(\frac{287}{\sqrt{Z}}\right) \qquad \textbf{(5)}$$

- From the above equations, the standard deviation of the deflection angle is directly related to Z, which is the basis for the muon tomography applications.
- At least, two muon trackers are necessary to detect muons entering and leaving the inspection volume and to measure the position and the direction of crossing particles.
- Applications of muon tomography are concentrated in the fields of nuclear security and safety, controls of transport, such as containers and trucks, for the detection of illicit or dangerous materials, etc.

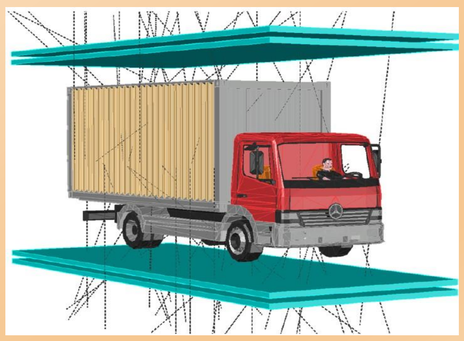

Figure 2: Cargo inspection using muon tomography [3].

4. The muography activities at NISER

- At NISER, we are developing a muon telescope, in modular form, for the applications in safety and geoscience. The telescope is comprise of four acrylic chambers, housing a resistive plate chambers (RPC) as the tracking detectors. The SolidWorks [4] diagram of the telescope is shown in ***Figure 3***, and that of the chamber is shown in ***Figure 4.***

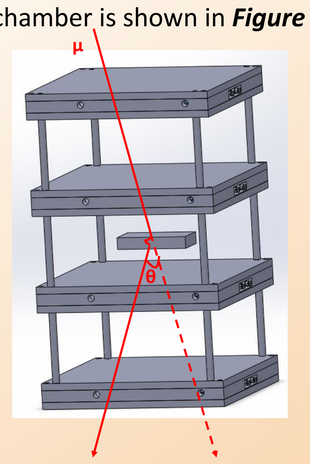

Figure 3: SolidWorks diagram of the muon telescope

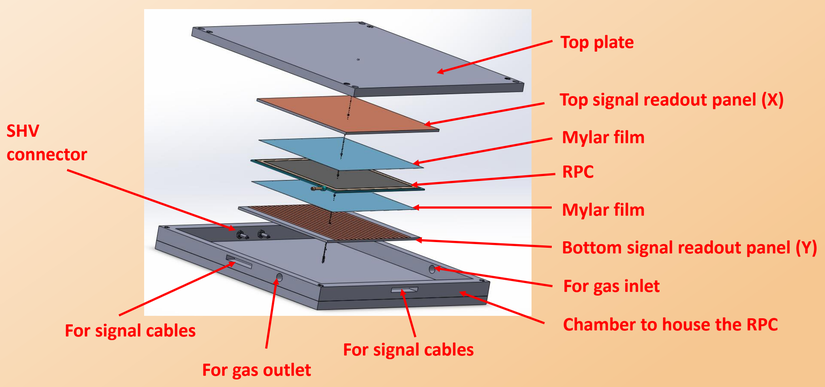

Figure 4: SolidWorks diagram of the chamber with all the components

- Resistive plate chambers (RPC) are parallel plate gaseous detectors, which work on the ionization principle. They are used in collider and neutrino physics experiments for the muon identification. The schematic of a single gap RPC is show in ***Figure 5***.

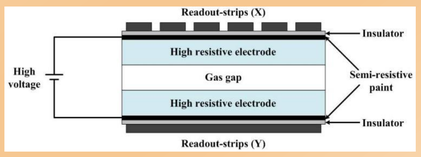

Figure 5: Schematic of a resistive plate chamber

5. Developing and testing the muon tracking detectors

- For this project, we chose the RPCs motivated by their simplicity in construction, cost-effectiveness in production, compact in size and excellence in performance metrics such as efficiency (95%), spatial (up to tens of μm) and time resolutions (up to tens of ps) [5].
- RPCs are developed using both Bakelite and float glass sheets of thickness 1.4 mm and 3 mm, respectively. A conductive coating is applied to the outer surfaces of the sheets. The surface resistance of the electrodes is ~ 1 MΩ/□. The active area of the RPC is 16 × 16 cm². The constructed glass RPC is shown in ***Figure 6.***

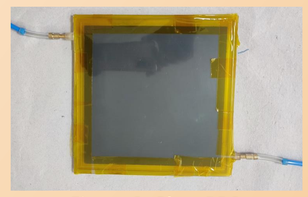

Figure 6: Glass RPC

- The efficiencies of the RPCs as function of the applied voltages are measured using the experimental set-up (schematic) shown in ***Figure 7***. The efficiencies are ~95% on the plateau region (***Figure 8***).

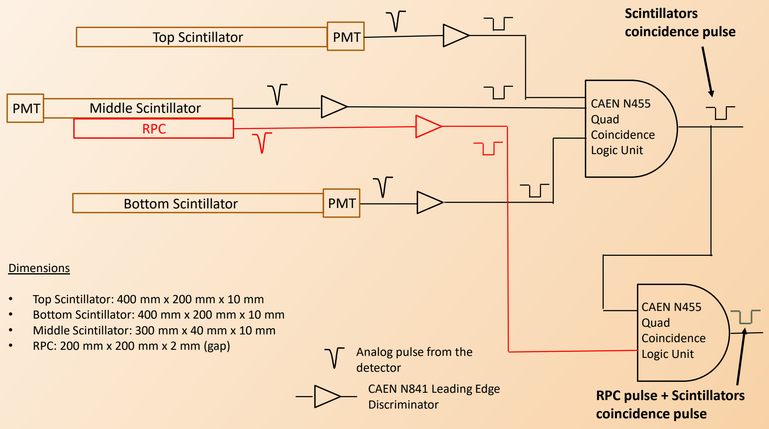

Figure 7: Experimental setup made to study the efficiencies of the RPCs.

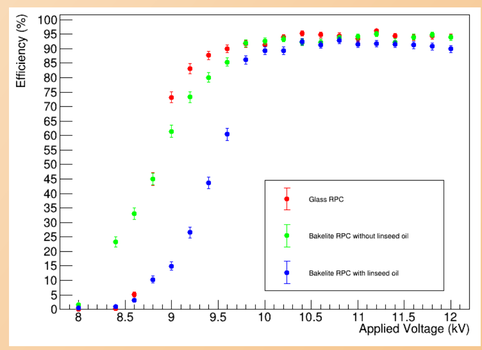

Figure 8: Efficiency of the RPCs as a function of applied voltage.

- The PCB based readout panels are developed to read the pulses from the RPCs. Each PCB has 16 strips with a pitch of 1 cm. Strip width is 0.9 cm and the gap between two consecutive strips is 0.1 cm.
- An acrylic chamber, to house the RPC, is developed at the NISER mechanical workshop.
- The readout panel placing inside the acrylic chamber are shown in ***Figure 9***.

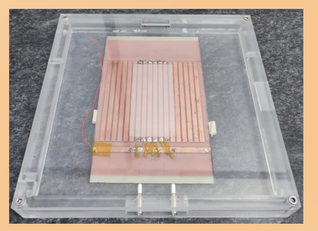

Figure 9: Readout panel placed inside the acrylic chamber.

Electronics:

- The RPCs are powered using the CAEN A7512DNB single channel power supply module (***Figure 10***). This module has the voltage and current ranges up to 12 kV and 20 μA, respectively.
- The RPCs pulses are analysed using a complete data acquisition system CAEN DT5550W (***Figure 11***), based on PETIROC ASICs and a programmable FPGA.

Figure 10: CAEN A7512DNB power supply module

Specifications of PETIROC ASIC:

- 32 input channels
- Positive or negative signal polarity
- Dynamic range: 0-480 pC
- 32 trigger outputs
- 40 ps bin TDC

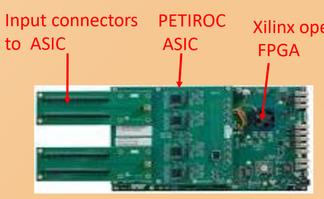

Figure 11: CAEN DT5550W

6. Simulations studies

- A muon telescope is designed using Geant4 simulation toolkit [6] with four acrylic chambers, where each chamber house an RPC as a tracking detector. EcoMug [7] is used to generate the cosmic-ray muon flux. The simulated muon tracks on the telescope are shown in ***Figure 12***.
- Point of Closest Approach (POCA) algorithm is developed to produce the image of the simulated lead block of the size 10 × 10 × 10 cm³ placed between the detectors D1 and D2. The reconstructed image of the lead block is shown in ***Figure 13.***
- **POCA algorithm**:
  - Find the minimum distance between the two tracks, from the upper and lower trackers, respectively.
  - POCA point is the mid point of line joining P_C and Q_C.
  - Reconstruction of the POCA points results in the reconstructed image.
  - The illustration is shown in the beside figure.

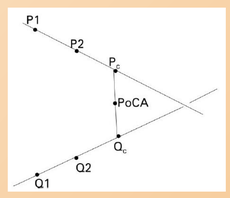

Illustration of POCA algorithm

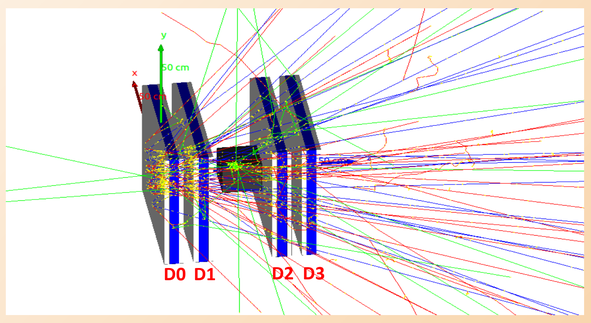

Figure 12: Simulated telescope geometry and the muon tracks.

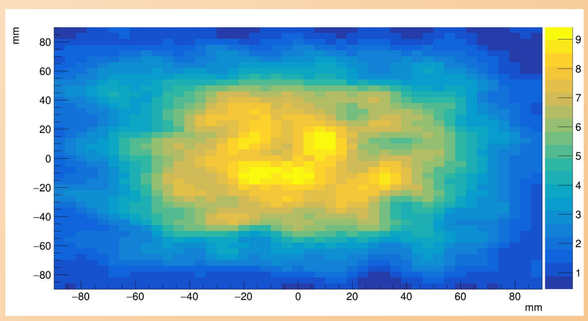

Figure 13: POCA image of the Lead block.

- The intrinsic angular resolution of the telescope is 2.8 mrad (***Figure 14***) and that while placing the 10 × 10 × 10 cm³ lead block is 13.8 mrad (***Figure 15***) , which is close to the theoretically calculated value of 12 mrad from equation **(4)**.

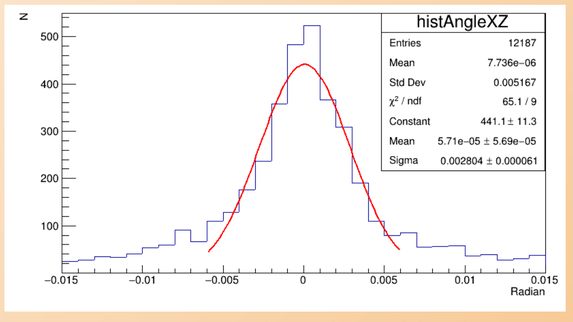

Figure 14: Intrinsic angular resolution of the telescope.

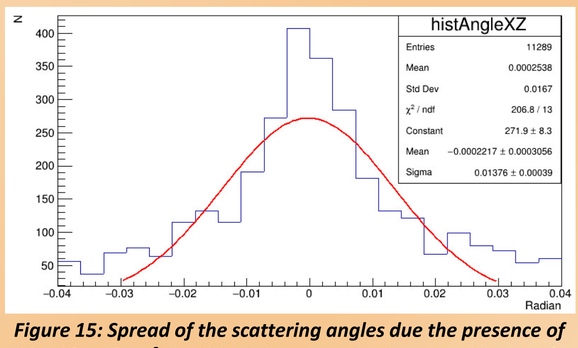

Figure 15: Spread of the scattering angles due the presence of 10 × 10 × 10 cm³ lead block between the detectors D1 and D2.

7. References

[1] G. Bonomi et. al., *prog. part. nucl. phys.* 112 (2020) 103768.
[2] *https://lingacom.com/*
[3] L. Bonechia, R. D'Alessandroa, A. Giammanco, *Rev. Phys.* 5 (2020) 100038.
[4] *https://www.solidworks.com*
[5] P. Fonte, *IEEE Trans. Nucl. Sci.* 49 (2002) 881.
[6] *https://geant4.web.cern.ch*
[7] D. Pagano et. al., *Nucl. Instrum. and Methods in Phys. Res., A* 1014 (2021) 165732